International Journal of Heat and Mass Transfer 52 (2009) 4525–4534

Contents lists available at ScienceDirect

International Journal of Heat and Mass Transfer

journal homepage: www.elsevier.com/locate/ijhmt

Direct numerical simulation for a time-developing natural-convection boundary layer along a vertical flat plate

Mohammad Zoynal Abedin [a], Toshihiro Tsuji [b,*], Yasuo Hattori [c]

[a] Department of Environmental Technology and Urban Planning, Graduate School of Engineering, Nagoya Institute of Technology, Gokiso-Cho, Showa-Ku, Nagoya 466-8555, Japan
[b] Department of Engineering Physics, Electronics and Mechanics, Graduate School of Engineering, Nagoya Institute of Technology, Gokiso-Cho, Showa-Ku, Nagoya 466-8555, Japan
[c] Fluid Science Sector, Central Research Institute of Electric Power Industry, 1646 Abiko, Abiko-shi, Chiba-ken 270-1194, Japan

ARTICLE INFO

Article history:
Received 11 July 2008
Received in revised form 7 November 2008
Accepted 13 March 2009
Available online 23 May 2009

Keywords:
Natural convection
Turbulent boundary layer
Direct numerical simulation
Transition
Heat transfer

ABSTRACT

Direct numerical simulations were performed for the transitional and turbulent natural-convection boundary layer for air and water along a hot vertical flat plate. The numerical results for water well reproduce the vortex-like structures as observed experimentally in the thermal field for a high Prandtl-number fluid. When the calculated values are evaluated with the integral thickness of the velocity boundary layer as a length scale, the turbulence statistics such as heat transfer rate, mean velocity, mean temperature, intensity of velocity and temperature fluctuations, Reynolds shear stress and turbulent heat fluxes correspond relatively well with those obtained from the experiments for space-developing flows. This shows that the time-developing direct numerical simulation of the natural-convection boundary layer can provide details that are difficult to obtain in experiments. These data are of great importance to understand the turbulence structures.

1. Introduction

The turbulent natural-convection boundary layer along a hot vertical flat plate serves as a basic example of the typical turbulence in thermally driven flows, which occur in many environmental, industrial and engineering applications. The analysis of this boundary layer is important not only to clarify the heat transfer mechanisms but also to evaluate the basic structures of turbulent buoyancy-driven flows.

The fundamental characteristics of the turbulent natural-convection boundary layer along a hot vertical plate, such as heat transfer rates, mean velocity and mean temperature profiles, were extensively investigated by many researchers [1–15]. In some of these studies advanced measurements and flow visualizations have been conducted using various experimental techniques. The turbulence characteristics of the natural-convection boundary layer turn out to differ from those observed in forced-convection boundary layers in several respects.

However, some essential features of the transitional and turbulent boundary layer are still not sufficiently understood due to the difficulty in obtaining reliable experimental data for all turbulence quantities. Therefore, it is expected that some lacking data in the experiments could be compensated for by applying numerical analyses. There are several numerical approaches for the turbulent natural-convection boundary layer [16–18], but all of them provide only turbulence statistics calculated with various turbulence models. Under such circumstances, it is impossible to reveal the turbulence structures in the natural-convection boundary layer.

Recently, direct numerical simulations have been actively utilized to analyze various flows and heat transfer phenomena and are of assistance to comprehend the turbulence characteristics. For forced convection, turbulent flows in channels and pipes have been extensively calculated using various numerical approaches, and the information difficult to be obtained in experiments are acquired for the velocity and thermal fields [19–22]. Also for natural convection, the direct numerical simulations of turbulent flows between two infinite, differentially heated vertical plates have been performed to evaluate the scaling behavior of turbulence statistics [23,24]. However, these studies only concern the internal flows satisfying the periodic boundary condition in the streamwise direction. If a direct numerical simulation is performed for external flows such as forced- and natural-convection boundary layers spatially developing in the streamwise direction, it requires a considerable computational effort. That is, the space-developing numerical approach needs huge storage capacity and computation time. Therefore, to reduce the computational effort significantly, instead of using the spatial approach, we simulated the turbulent natural-convection boundary layer along a hot vertical plate under time-developing conditions. Although the time-developing approach was employed to simulate a decelerated wall-bounded shear flow [25], hypersonic turbulent boundary layers [26] and so on, no direct numerical simulation has so far been conducted for the turbulent natural-convection boundary layer along a hot vertical plate (neither with the

* Corresponding author. Tel./fax: +81 52 735 5333.
E-mail address: tsuji.toshihiro@nitech.ac.jp (T. Tsuji).

0017-9310/$ - see front matter © 2009 Elsevier Ltd. All rights reserved.
doi:10.1016/j.ijheatmasstransfer.2009.03.061

Nomenclature

c_p	specific heat at constant pressure, kJ/(kg K)
g	gravitational acceleration, m/s^2
Gr_δ	Grashof number based on integral thickness δ, $\frac{g\beta\Delta T_w\delta^3}{\nu^2}$
h	heat transfer coefficient, W/(m^2 K)
Nu_δ	Nusselt number based on integral thickness δ, $h\delta/k$
p	pressure, Pa
Pr	Prandtl number, $\mu c_p/k$
Re_δ	Reynolds number based on integral thickness δ, $U_\infty\delta/\nu$
T	mean temperature, °C
t	instantaneous temperature, °C
t'	temperature fluctuation, °C
U	mean streamwise velocity, m/s
u	instantaneous streamwise velocity, m/s
u'	streamwise velocity fluctuation, m/s
u_i	instantaneous velocity in x_i direction, m/s
v	instantaneous transverse velocity, m/s
v'	transverse velocity fluctuation, m/s
w	instantaneous spanwise velocity, m/s
x	distance from leading edge of flat plate, m
x_i	coordinate in tensor notation, m
y	distance from wall, m
z	spanwise distance, m

Greek symbols

α	thermal diffusivity, m^2/s
β	coefficient of volume expansion, 1/K
ΔT_w	temperature difference between wall and ambient, $T_w - T_\infty$, °C
δ	integral thickness of the velocity boundary layer, $\int_0^\infty U/U_m dy$, m
δ_θ	integral thickness of the thermal boundary layer, $\int_0^\infty \theta dy$, m
θ	dimensionless temperature, $(t - T_\infty)/\Delta T_w$
k	thermal conductivity, W/(m K)
μ	viscosity, Pa s
ν	kinematic viscosity, m^2/s
ρ	density, kg/m^3
τ	time, s
τ_w	wall shear stress, Pa
ω	vorticity component in spanwise direction, 1/s

Superscripts

*	normalized variables with δ_0 and ν
¯	time-averaged quantities for experimental statistics and ensemble-averaged quantities for analytical results

Subscripts

m	maximum value
w	wall condition
0	initial condition
∞	ambient condition

spatial nor with the temporal approach). The numerical results will provide information that is very difficult to obtain from experiments. However, structures found from time-developing flows still need to be properly converted to those relevant for space-developing flows.

In the present study, time-developing direct numerical simulations for the turbulent natural-convection boundary layers both for air and water along a hot vertical flat plate have been performed. By employing the integral thickness of the velocity boundary layer as a length scale, the numerical results are compared with the turbulence statistics experimentally obtained by Tsuji and Nagano [10–12] for air and by Tsuji and Kajitani [15] for water in the space-developing boundary layer. In this way, it is confirmed that the turbulence characteristics of the space-developing natural-convection boundary layer can be predicted to some extent with a time-developing direct numerical simulation.

2. Numerical procedure

We consider the time-developing boundary layer flow induced by heating an infinitely long vertical flat surface at a uniform temperature from a given time onward. The calculation domain and coordinates are shown in Fig. 1. The coordinates in the vertical, wall-normal and spanwise directions are x, y and z, respectively, and the instantaneous velocities u, v and w are specified in the relevant directions. The symbol δ_0 is the initial value of the integral thickness of the velocity boundary layer. As will be described in more detail below, this initial value represents the laminar boundary layer. The wall and ambient temperatures, T_w and T_∞, are assumed to be constant. The boundary layer thickness develops over time from about $4\delta_0$ in the laminar flow regime to about $40\delta_0$ in the turbulent flow regime. Therefore, the computational domain is set up as $20\pi\delta_0$, $60\delta_0$ and $20\pi\delta_0$ in the x, y and z directions, respectively.

The dimensionless governing equations expressing the conservation of mass, momentum and energy with the Boussinesq approximation can be written in the tensor notation as follows:

$$\frac{\partial u_i^*}{\partial x_i^*} = 0 \tag{1}$$

$$\frac{\partial u_i^*}{\partial \tau^*} + u_j^*\frac{\partial u_i^*}{\partial x_j^*} = -\frac{\partial p^*}{\partial x_i^*} + \frac{\partial^2 u_i^*}{\partial x_j^{*2}} + Gr_{\delta_0}\theta \tag{2}$$

$$\frac{\partial \theta}{\partial \tau^*} + u_j^*\frac{\partial \theta}{\partial x_j^*} = \frac{1}{Pr}\frac{\partial^2 \theta}{\partial x_j^{*2}} \tag{3}$$

Here, $Gr_{\delta_0} = g\beta\Delta T_w{\delta_0}^3/\nu^2$ is the Grashof number based on δ_0, the superscript '*' denotes variables that have been made dimensionless with δ_0 and ν, and θ is the dimensionless temperature defined as $\theta = (t - T_\infty)/\Delta T_w$.

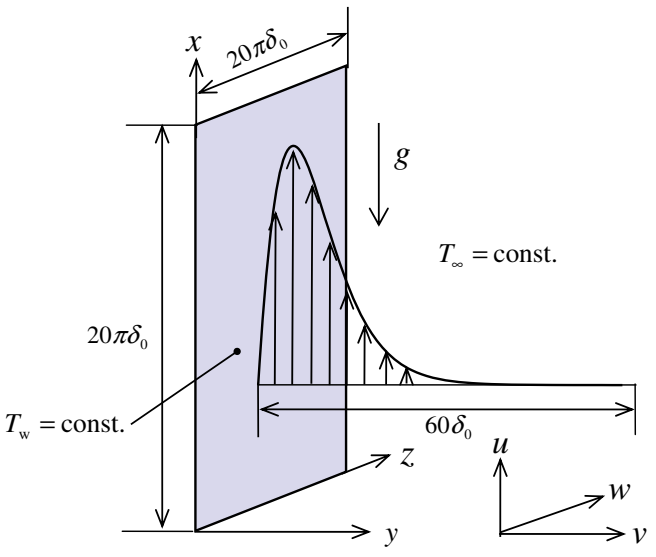

Fig. 1. Calculation domain and coordinates.

Periodic boundary conditions are applied for the x^* and z^* directions and the boundary condition in the y^* direction is provided as follows:

$$y^* = 0: \quad u^* = v^* = w^* = 0, \quad \theta = 1,$$
$$y^* = 60: \quad u^* = v^* = w^* = \theta = 0 \tag{4}$$

The momentum and energy equations were discretized by the second-order accurate central difference scheme on staggered grids. The calculation of the flow field was advanced with a fractional-step method. The second-order Adams–Bashforth time discretization scheme was adopted to calculate the convective and advective terms and the second-order Crank–Nicolson scheme was used for the viscous, diffusion and buoyancy terms. A nonuniform grid was employed in the y^* direction and uniform grids were used in the x^* and z^* directions. The calculations were mainly conducted with $(128, 200, 128)$ grid points in the (x^*, y^*, z^*) directions and the dimensionless time step was set to 2×10^{-5}. The numerical calculation was carried out on the INTEL CORE 2 QUAD EXTREME processor of speed 2.66 GHz and the computation time was about 40 h to accomplish fully developed turbulence (the number of time steps was set to 102,400).

At the beginning of the calculation, the laminar velocity and temperature profiles were given as initial values. For the time-developing laminar boundary layer on an infinite flat plate, the analytical solutions under the various thermal boundary conditions were given in tabular form by Schetz and Eichhorn [27]. After the temperature of the vertical wall has been instantaneously increased from $\theta = 0$ to $\theta = 1$ at time zero, the velocity and temperature profiles can be expressed as follows:

$$Pr \neq 1: \quad u^* = \frac{4Gr_{\delta_0}\tau^*}{1-Pr}\left[i^2\mathrm{erfc}\ (\eta) - i^2\mathrm{erfc}\left(\frac{\eta}{\sqrt{Pr}}\right)\right] \tag{5}$$
$$Pr = 1: \quad u^* = 2Gr_{\delta_0}\tau^*\eta\ \mathrm{ierfc}\ (\eta) \tag{6}$$
$$\theta = \mathrm{erfc}(\eta) \tag{7}$$

Here, $\eta = y/2\sqrt{\alpha\tau}$ and $\mathrm{erf}(\eta)$ is the error function of η, $\mathrm{erfc}\ (\eta) = 1 - \mathrm{erf}\ (\eta)$, $\mathrm{ierfc}\ (\eta) = \exp(-\eta^2)/\sqrt{\pi} - \eta\ \mathrm{erfc}\ (\eta)$ and $\mathrm{i}^2\mathrm{erfc}\ (\eta) = (1/4)[\mathrm{erfc}\ (\eta) - 2\eta\ \mathrm{ierfc}\ (\eta)]$. Eqs. (5) and (7) were used as the initial profiles of the laminar boundary layer at $Gr_{\delta 0} = 3000$ and very small disturbances were added to induce the transition to turbulence.

In general, the calculated results for time-developing flows cannot directly be compared with those obtained for space-developing flows. To make a meaningful comparison, an appropriate length scale that is common for both flows is required. Therefore, we adopted the integral thickness of the velocity boundary layer δ as a length scale defined by:

$$\delta = \int_0^\infty U/U_\mathrm{m} dy \tag{8}$$

Here U is the mean velocity, found by averaging the velocity in the $(x–z)$ plane, and U_m is the maximum mean velocity in the boundary layer. This length scale δ was previously used by Vliet and Liu [4] and Tsuji and Nagano [12] to present experimental results of the natural-convection boundary layer.

Before showing the numerical results for the turbulent boundary layer, we determine the suitability of a correlation with the integral thickness of the velocity boundary layer for the space- and time-developing laminar boundary layers. The dimensionless velocity profile $(u\delta/\nu)/Gr_\delta$ and the dimensionless temperature profile θ are shown against y/δ in Fig. 2 for the laminar boundary layer of air ($Pr = 0.71$). The relation between $(ux/\nu)/Gr_x^{1/2}$ and $(y/x)/Gr_x^{1/4}$ (here, x is based on the distance from the leading edge of a hot vertical plate), which is often used to express the similarity of the laminar velocity profile in the space-developing boundary layer, is equivalent to the coordinates shown in Fig. 2.

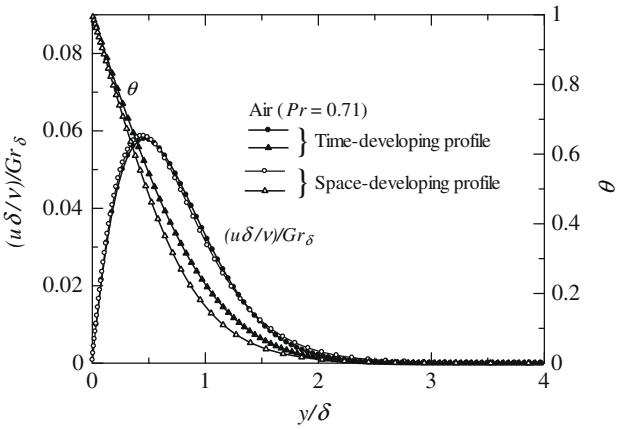

Fig. 2. Velocity and temperature profiles in the laminar boundary layer for air ($Pr = 0.71$).

As can be seen in Fig. 2, the velocity and temperature profiles for the time-developing laminar boundary layer in air correspond well with those for the space-developing laminar boundary layer. Note that the difference in the temperature profiles between the time- and space-developing flows becomes much smaller when the integral thickness of the thermal boundary layer $\delta_\theta = \int_0^\infty \theta dy$ is used to normalize y in the abscissa axis. However, the discrepancy between the velocity profiles of the time- and space-developing flows arises with use of δ_θ.

Thus, it is anticipated that the direct numerical simulation of the time-developing boundary layer will provide relevant information about the turbulence characteristics of the natural-convection boundary layer, when the numerical results are presented with the integral thickness of the velocity boundary layer as a length scale.

3. Results and discussion

Direct numerical simulations were conducted by adding various initial disturbances having less than 1% of the intensity of the streamwise velocity fluctuations observed in the turbulent boundary layer. However, these small initial disturbances had a significant effect on the calculated results. In fact, the turbulent statistics obtained by averaging instantaneous quantities over the $(x^*–z^*)$ planes parallel to the wall depend on the initial disturbances. Therefore, we show the following turbulence statistics as ensemble averaged values of several iterations with different initial disturbances and compare them with the experimental results for the space-developing flows by employing the integral thickness of the velocity boundary layer. The calculations were also performed by using both the double number of grid points in the x or z direction and the half of the time step, but there is a little difference among these results, such as for the fluctuation of turbulent statistics averaged over the $(x^*–z^*)$ planes parallel to the wall.

3.1. Heat transfer rate, wall shear stress and transition behavior

Simulation results for the wall heat transfer in the natural-convection boundary layer along a hot vertical plate for air ($Pr = 0.71$) and water ($Pr = 6.0$), for laminar, transitional and turbulent conditions, are compared with available experimental data in Fig. 3. Shown is the relation between the Nusselt number Nu_δ and the Grashof number Gr_δ based on the integral thickness δ. In the laminar region, Nu_δ values for the time-developing flow become somewhat lower than those for the space-developing flow, namely $Nu_\delta = 0.96$ versus $Nu_\delta = 1.09$ for air, and $Nu_\delta = 1.76$ versus $Nu_\delta = 2.08$ for water, respectively. If the Nusselt number is evalu-

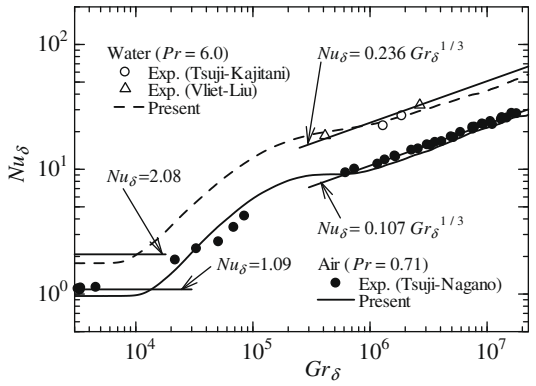

Fig. 3. Heat transfer rates in the natural-convection boundary layer (δ) for air (Pr = 0.71) and water (Pr = 6.0).

ated with the integral thickness of the thermal boundary layer δ_θ, the difference between the values for the space- and time-developing flows becomes smaller, as previously mentioned for the temperature profile shown in Fig. 2.

The transition behavior in air corresponds well with the experimental data of Tsuji and Nagano [10]. In the turbulent region, Nu_δ for air varies proportionally to $Gr_\delta^{1/3}$, and agrees well with the empirical formula $Nu_\delta = 0.107 Gr_\delta^{1/3}$ proposed by Tsuji and Nagano [10]. On the other hand, the Nusselt number in the turbulent region for water coincides well with the experimental data (Vliet and Liu [4], Tsuji and Kajitani [15]) and is relatively close to the empirical formula $Nu_\delta = 0.236 Gr_\delta^{1/3}$ suggested by Fujii et al. [5] for natural convection along a vertical circular surface. It should be noted that the critical Grashof number based on the integral thickness of the velocity boundary layer, which indicates the transition to turbulence, is about 10^4 both for air and water.

The dimensionless wall shear stresses of the turbulent natural-convection boundary layers both in air and water are presented in Fig. 4, which shows $\tau_w/(\rho g\beta \Delta T_w \delta)$ versus Gr_δ. In the laminar region for air, the wall shear stress becomes slightly lower than that for the space-developing flow, namely $\tau_w/(\rho g\beta \Delta T_w \delta) = 0.306$ versus $\tau_w/(\rho g\beta \Delta T_w \delta) = 0.313$. When the transition to turbulence occurs, the value of wall shear stress gradually approaches the empirical formula $\tau_w/(\rho g\beta \Delta T_w \delta) = 1.01 Gr_\delta^{-2/9}$ in the turbulent region proposed by Tsuji and Nagano [10], although it becomes somewhat larger than the measurements. This discrepancy may be related to the peculiar turbulence characteristics experimentally observed very near the wall of the natural-convection boundary layer [13], which will be mentioned later. The wall shear stress for water varies in a similar way as for air, but some discrepancy between the time- and space-developing flows appears in the laminar region, namely $\tau_w/(\rho g\beta \Delta T_w \delta) = 0.260$ versus $\tau_w/(\rho g\beta \Delta T_w \delta) = 0.227$.

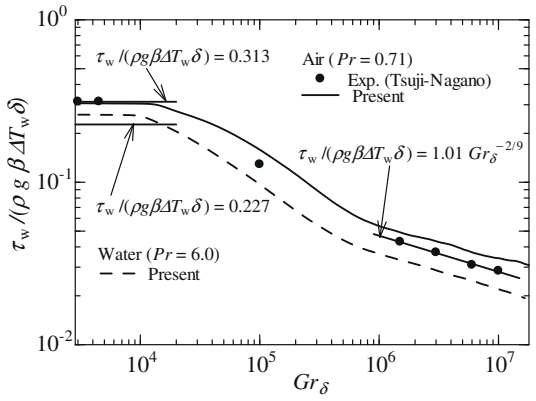

Fig. 4. Wall shear stresses in the natural-convection boundary layer for air (Pr = 0.71) and water (Pr = 6.0).

For the transition behavior of the natural-convection boundary layer in water, the variations of the isotherms and vorticity in the (x^*–y^*) plane obtained from the direct numerical simulation are presented in Fig. 5(a). Fig. 5(b) shows the transition behavior of the thermal boundary layer in spindle oil ($Pr \approx 70$) experimentally observed with an optical method by Fujii et al. [5]. Despite the difference in Prandtl number, the variations of the thermal field for water and spindle oil bear a close resemblance with each other, i.e. with the progress of transition, the thermal boundary layer shows the shedding of plumes whereas periodic vortex-like excitations occur in the outer region of the boundary layer. Finally the whole of the thermal field changes to turbulence. Fujii et al. [5] suggested that a similar transition behavior would also emerge in water, and that is exactly what the direct numerical simulation shows. However, such periodic vortex-like excitations do not clearly appear in the calculated results for air and the vorticity is distributed irregularly after the commencement of the transition (not shown in the figure). Consequently, the transition to turbulence in air seems to be more rapid than that in water, which may result from the difference between the thickness of the thermal boundary layers in air and water against the thickness of the velocity boundary layer. The appearance of vortex-like excitations in the thermal boundary layer is expected to become more pronounced for high Prandtl-number fluids.

3.2. Mean velocity and temperature profiles

The profiles of the mean velocity in the natural-convection boundary layer for air, normalized by the maximum mean velocity U_m, are plotted in Fig. 6, and they are compared with the measurements for the space-developing flow by Tsuji and Nagano [11]. The abscissa is the dimensionless wall-normal distance y/δ. The velocity profiles calculated at those Grashof numbers that approximately correspond to the experiment agree very well with the experimental data in the turbulent boundary layer. The predictions for the mean temperature profiles in the natural-convection boundary layer in air normalized by ΔT_w are compared with the measurements of Tsuji and Nagano [11] in Fig. 7. Again, the agreement is very good.

The predicted and measured mean velocity and mean temperature distributions in the natural-convection boundary layer in water are shown in Figs. 8 and 9, respectively. Note that the mean velocity profile measured by Tsuji and Kajitani [15] has no data points very near to the wall due to the difficulty of obtaining such data with a PIV (particle image velocimetry). The agreement between the calculations and measurements for the velocity and thermal fields is relatively good when choosing approximately the same Grashof number.

3.3. Intensities of velocity and temperature fluctuations

The intensities of the velocity fluctuations u' and v', normalized by the maximum mean velocity U_m, in the turbulent boundary layer both in air and water are shown in Figs. 10 and 11, respectively. Comparison is made with the measurements of Tsuji and Nagano [11] for air and Tsuji and Kajitani [15] for water. Although there exists some discrepancies between the calculations and the measurements for the wall-normal velocity component very near to the wall, the general shapes of these profiles are in good agreement. For example, the maximum intensity of these velocity fluctuations occurs at the location $y/\delta \approx 0.8$ beyond the maximum mean velocity location.

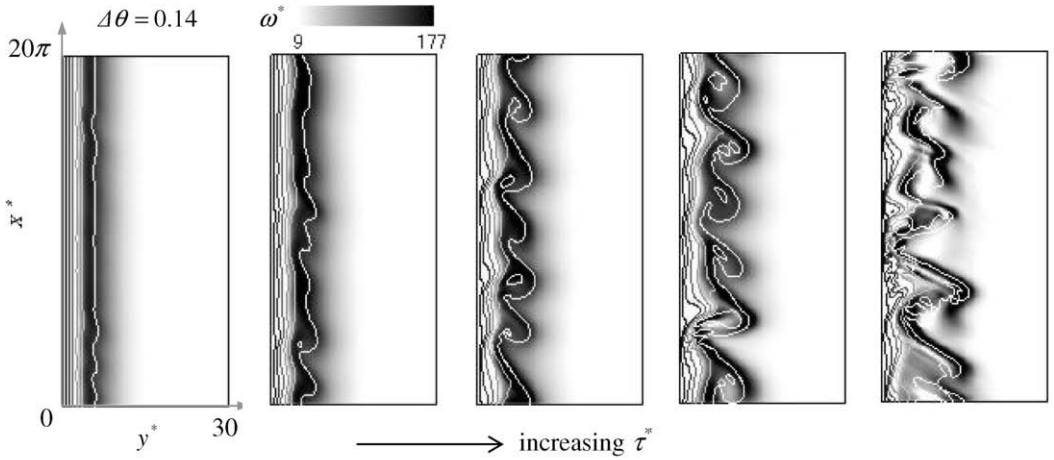

(a) Isotherms and contours of iso-vorticity obtained with direct numerical simulations for water

$(Pr = 6.0, Gr_\delta = 1.03\times10^3 \sim 2.92\times10^4)$

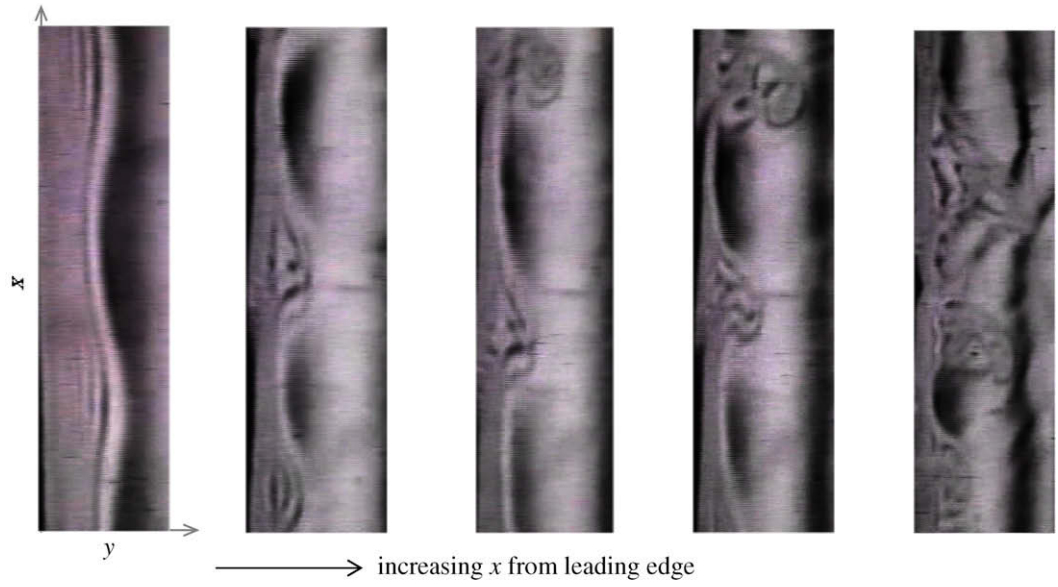

(b) Isotherms in the experiment of Fujii et al. [5] for spindle oil

$(Pr \approx 70, Gr_x = 1.03\times10^3 \sim 2.92\times10^4)$

Fig. 5. Visualization of the transition process in the (x–y) plane.

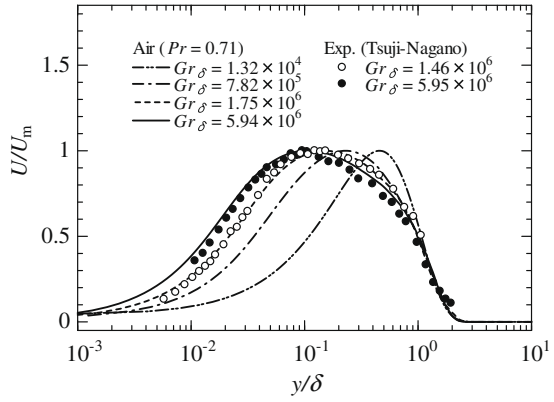

Fig. 6. Mean velocity profiles from laminar to turbulence for air (Pr = 0.71).

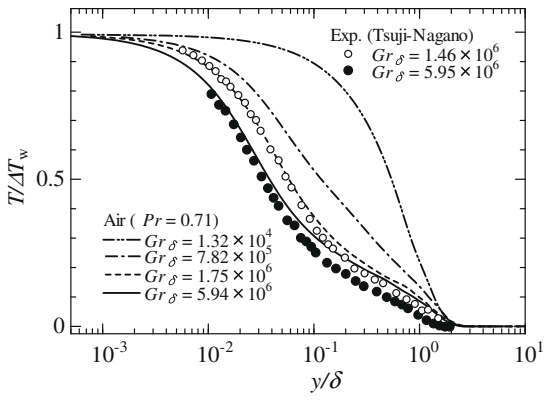

Fig. 7. Mean temperature profiles from laminar to turbulence for air (Pr = 0.71).

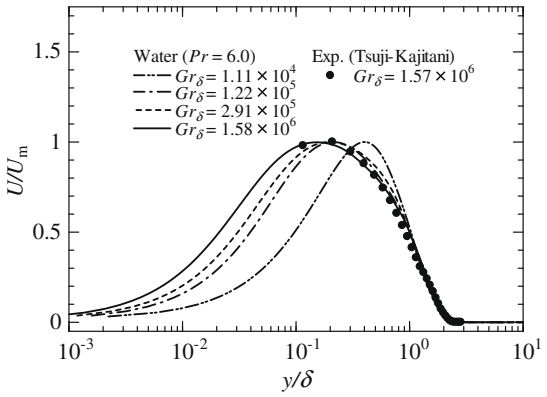

Fig. 8. Mean velocity profiles from laminar to turbulence for water ($Pr = 6.0$).

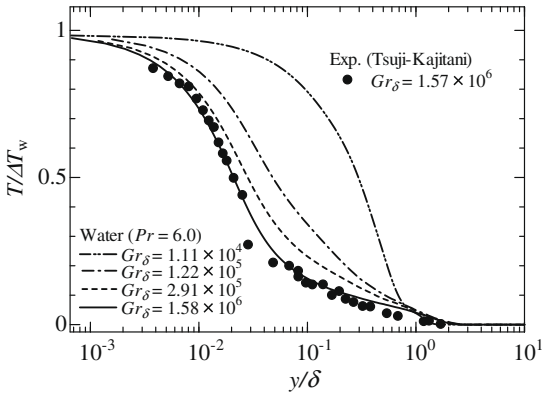

Fig. 9. Mean temperature profiles from laminar to turbulence for water ($Pr = 6.0$).

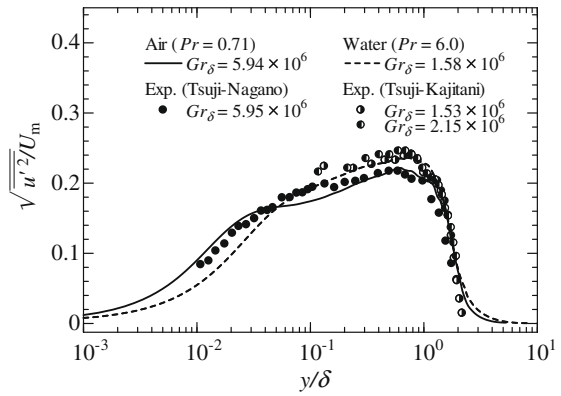

Fig. 10. Profiles of the intensity of streamwise velocity fluctuations for air ($Pr = 0.71$) and water ($Pr = 6.0$).

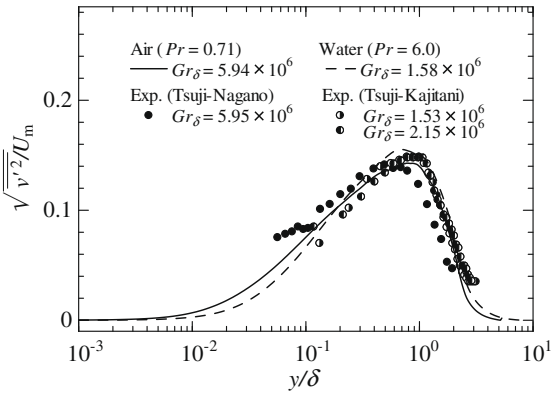

Fig. 11. Profiles of the intensity of wall-normal velocity fluctuations for air ($Pr = 0.71$) and water ($Pr = 6.0$).

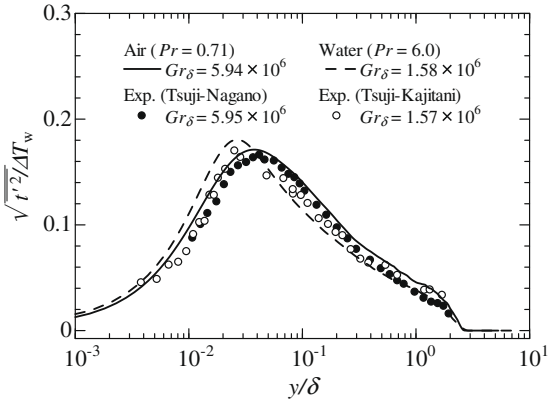

Fig. 12. Profiles of the intensity of temperature fluctuations for air ($Pr = 0.71$) and water ($Pr = 6.0$).

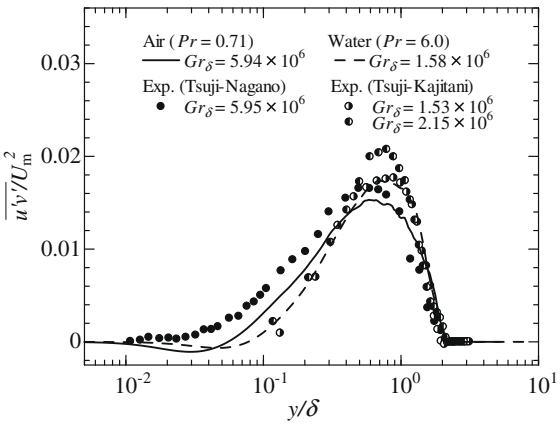

Fig. 13. Profiles of Reynolds shear stresses for air ($Pr = 0.71$) and water ($Pr = 6.0$).

Fig. 12 presents the intensity of the temperature fluctuation t' in the turbulent boundary layer both for air and water. The direct numerical simulations agree with the experimental results of Tsuji and Nagano [11] for air and of Tsuji and Kajitani [15] for water.

3.4. Reynolds shear stress and turbulent heat fluxes

The profiles of the Reynolds shear stress $\overline{u'v'}$ both in air and water normalized with the maximum mean velocity U_m are shown in Fig. 13. The calculated values reasonably agree with the experimental data (Tsuji and Nagano [11] for air and Tsuji and Kajitani [15] for water) over the whole boundary layer region. In the near-wall region, however, the numerical values become slightly negative, whereas the measurements are nearly zero. As suggested in the report of Tsuji et al. [13], there are peculiar characteristics in the turbulent natural-convection boundary layer such that the direct conversion from thermal energy to mechanical energy caused by the velocity–pressure gradient correlation may contribute to the generation of turbulent energy in the near-wall region. Therefore, it is conjectured that the discrepancy between the calculated values and measurements near the wall cannot be compensated for when the Boussinesq approximation is used in the governing

equations in direct numerical simulations. Instead, some other numerical approaches may be needed. A similar profile in which the Reynolds shear stress becomes negative near to the wall is numerically obtained by Peeters and Henkes [18], who solved the governing equations under the Boussinesq approximation with Reynolds stress and turbulent heat flux equations incorporating turbulence models.

Figs. 14 and 15 compare the numerically obtained results for the dimensionless turbulent heat fluxes both in air and water with the measurements (Tsuji and Nagano [11] for air and Tsuji and Kajitani [15] for water). As seen in Fig. 14, the simulation of the turbulent heat flux $\overline{v't'}$ in the wall-normal direction shows a similar behavior as the experimental results, and it is distinctively found that the turbulent heat flux for water becomes much smaller than that for air. This is due to an increase in the difference between the turbulence scales in the velocity and thermal fields for water of high Prandtl number, and consequently indicates a decrease of heat transport accompanied with turbulent fluid motions.

For the streamwise turbulent heat flux $\overline{u't'}$ as shown in Fig. 15, both the calculated and experimental results for water become much smaller than those for air in the outer region beyond the maximum mean velocity location. However, a clear distinction between the calculated and experimental results is observed for air in the near-wall region. The profile obtained from the direct numerical simulation obviously has negative values, while measurements become almost zero. A similar profile of the streamwise turbulent heat flux can be also seen in the numerical study of Peeters and Henkes [18]. This distinction may be attributed to the peculiar characteristics in the near-wall region of the turbulent natural-convection boundary layer as previously described for the behavior of Reynolds shear stress. On the other hand, the numerical results for water never show negative values, though it is not fully clear why they cannot become negative as in the case of air. Such a behavior of the streamwise turbulent heat flux for water, having a high Prandtl number, may be caused by the interacting turbulent velocity and temperature fluctuations having fairly different scales.

3.5. Observation of fluctuating velocity and thermal fields

The fluctuating streamwise velocity and temperature in the (y^*–z^*) plane, for both air and water, are displayed in Figs. 16 and 17, respectively. As shown in Fig. 16(a) and (b), the contours of the fluctuating streamwise velocity for air are well correlated with those of the temperature in the outer region beyond the maximum mean velocity location ($y^* \approx 4.6$). This is consistent with the profile of streamwise turbulent heat flux shown in Fig. 15. In contrast to this, the correlation between velocity and temperature contours

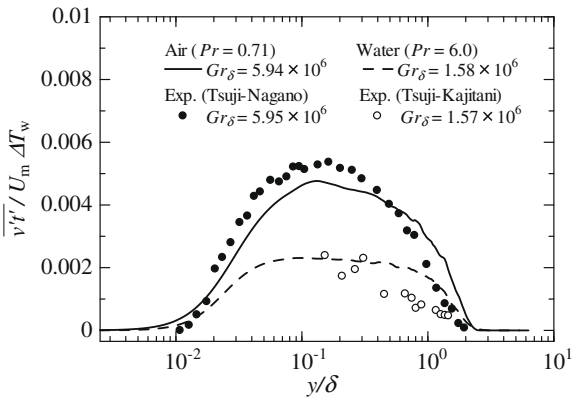

Fig. 14. Profiles of wall-normal turbulent heat fluxes for air ($Pr = 0.71$) and water ($Pr = 6.0$).

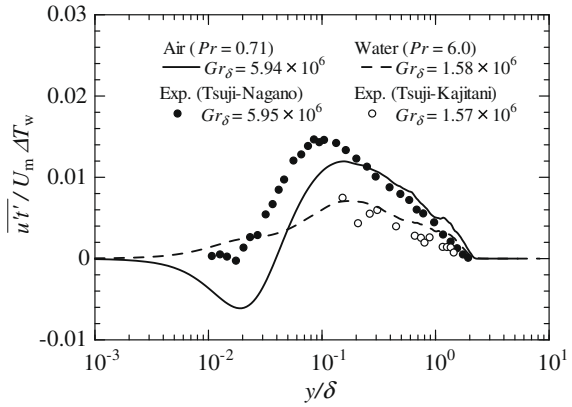

Fig. 15. Profiles of streamwise turbulent heat fluxes for air ($Pr = 0.71$) and water ($Pr = 6.0$).

for water is poor over the whole boundary layer as seen in Fig. 17(a) and (b). The contours of the fluctuating temperature for water, as shown in Fig. 17(b), obviously become small in scale and disperse over the whole boundary layer region compared with those for air shown in Fig. 16(b).

The contours of the fluctuating streamwise velocity and temperature in the (x^*–z^*) plane for both air and water, as observed near the maximum mean velocity location ($y/\delta \approx 0.07$), are depicted in Figs. 18 and 19, respectively. The high- and low-speed regions in the velocity field for air spindle in the streamwise direction as seen in Fig. 18(a), while those for water intersect in a different way as seen in Fig. 19(a). Such behavior becomes more pronounced near to the wall (not shown in the figure). On the other hand, the contours of the fluctuating temperature for water reveal much more dispersion in the (x^*–z^*) plane as shown in Fig. 19(b). This indicates that the average streamwise turbulent heat flux for water will become lower than for air, as was indeed found in Fig. 15.

4. Conclusions

As shown in the present study, time-developing direct numerical simulations with the Boussinesq approximation in the governing equations can give a general feature of the turbulent characteristics of the natural-convection boundary layer along a hot vertical plate, except for the behavior very near to the wall. The time-developing approach as applied here is much more computationally efficient compared to the space-developing approach. More advanced direct numerical simulations on the basis of the exact governing equations without the Boussinesq approximation are required to provide numerical results consistent with the experiments very close to the wall.

The following observations are made:

(1) When the integral thickness of the velocity boundary layer δ is used as a characteristic length scale, the calculated results obtained with time-developing direct numerical simulations can be correlated with measurements for space-developing flows.
(2) Both in the direct numerical simulations and the experiments, the transition to turbulence in the natural-convection boundary layer occurs at a Grashof number Gr_δ of approximately 10^4 both for air and water. The critical Grashof number indicating the transition to turbulence depends only slightly on the initial disturbances added to the laminar boundary layer in the direct numerical simulations.

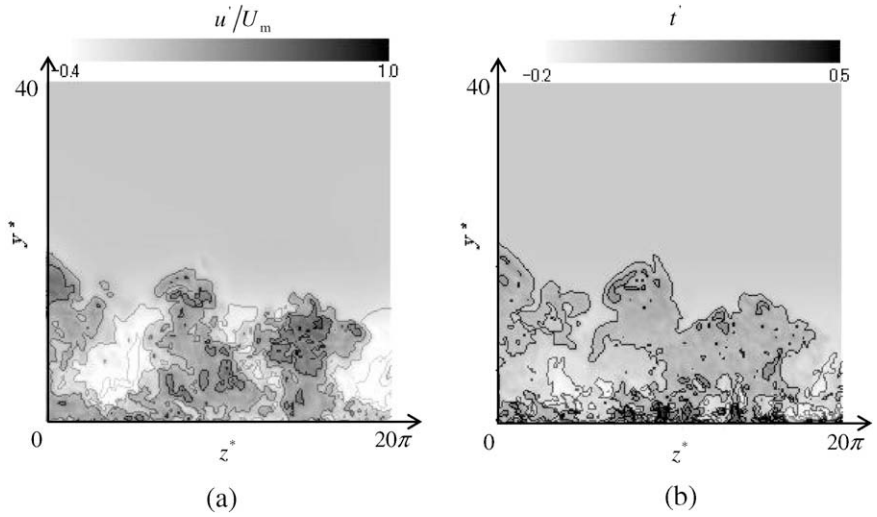

Fig. 16. Contours of the fluctuating temperature and velocity for air in the (y^*–z^*) plane ($Pr = 0.71$, $Gr_\delta = 3.98 \times 10^6$).

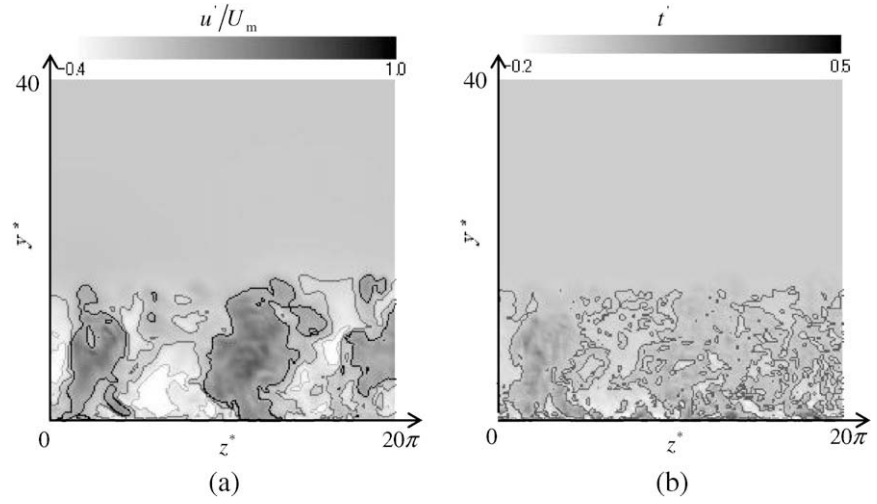

Fig. 17. Contours of the fluctuating temperature and velocity for water in the (y^*–z^*) plane ($Pr = 6.0$, $Gr_\delta = 4.02 \times 10^6$).

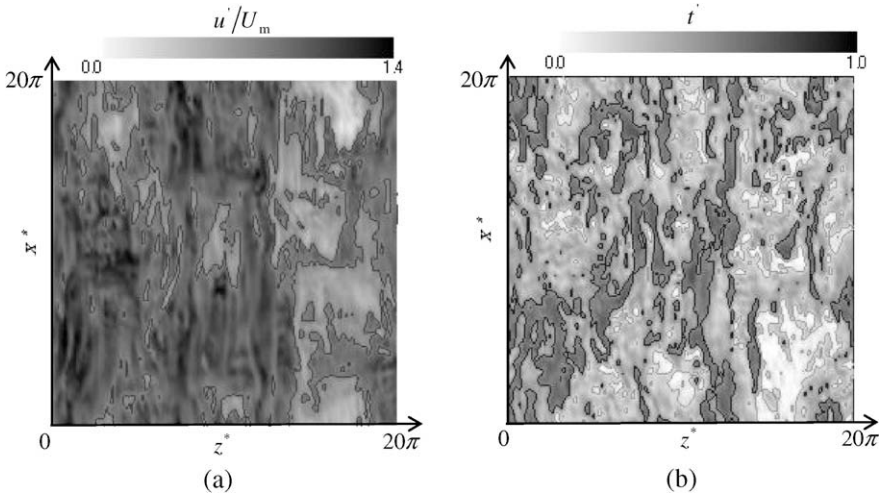

Fig. 18. Fluctuating temperature and velocity distribution for air in the (x^*–z^*) plane near the wall ($Pr = 0.71$, $Gr_\delta = 3.98 \times 10^6$, $y/\delta = 0.07$).

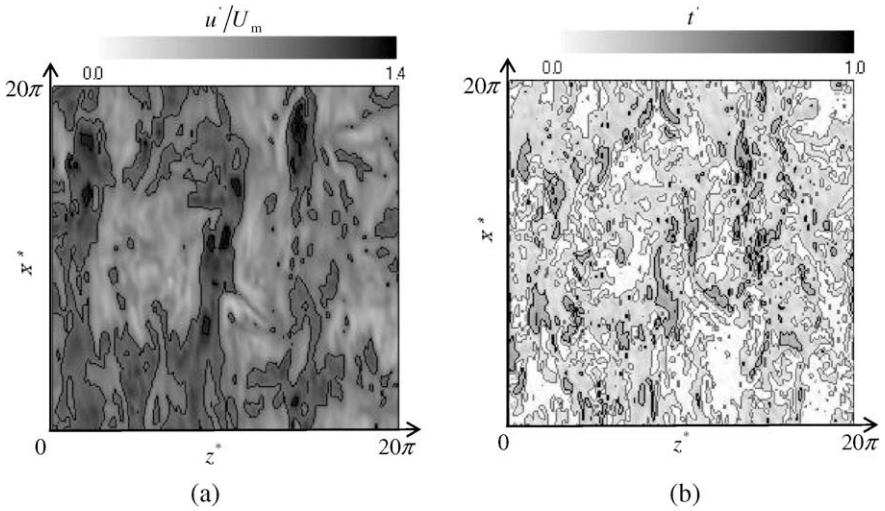

Fig. 19. Fluctuating temperature and velocity distributions for water in the (x^+–z^+) plane near the wall (Pr = 6.0, $Gr_\delta = 4.02 \times 10^6$, y/δ = 0.07).

(3) When the transition progresses, the thermal boundary layer in water shows the shedding of plumes and also vortex-like excitations occur, until finally the whole of thermal field changes to turbulence. Such a transition behavior agrees well with the experiments for high Prandtl-number fluid. However, the vortex-like excitations do not clearly appear in the simulation results for air.

(4) For the turbulent natural-convection boundary layer of both air and water, numerical statistics such as heat transfer rate, wall shear stress, mean velocity and mean temperature profiles, intensity of velocity and temperature fluctuations and Reynolds shear stress all agree fairly well with the experimental data.

(5) The difference in the turbulence characteristics between air and water occurs most clearly in the turbulent heat fluxes. The turbulent heat fluxes for water become much smaller than those for air due to the effect of the high Prandtl number. However, the direct numerical simulations might lack accuracy here, as the Boussinesq approximation was used, which seems to cause that the calculated streamwise turbulent heat flux in air differs from the measurements in the near-wall region.

Acknowledgements

The authors express their gratitude to Professor T. Fujii and Professor M. Fujii, Kyushu University, who deigned to offer precious video pictures for the transition of the natural-convection boundary layer in spindle oil. Also, the authors are thankful to Mr. Y. Saiki, H. Kimura, Y. Imoto and H. Kubo, students of Nagoya Institute of Technology, for their cooperation.

References

[1] C.Y. Warner, V.S. Arpaci, An experimental investigation of turbulent natural convection in air at low pressure along a vertical heated flat plate, Int. J. Heat Mass Transfer 11 (3) (1968) 397–406.
[2] R. Cheesewright, Turbulent natural convection from a vertical plane surface, Int. J. Heat Transfer 90 (1968) 1–8.
[3] A. Pirovano, S. Viannay et M. Jannot, Convection naturelle en regime turbulent le long d'une plaque plane verticale, in: Proceedings of the 9th International Heat Transfer Conference, Natural Convection, Elsevier, Amsterdam, vol. 4, NC 1.8, 1970, pp. 1–12.
[4] G.C. Vliet, C.K. Liu, An experimental study of turbulent natural convection boundary layers, Trans. ASME J. Heat Transfer C-91 (1969) 517–531.
[5] T. Fujii, M. Takeuchi, M. Fujii, K. Suzaki, H. Uehara, Experiments on natural-convection heat transfer from the outer surface of a vertical cylinder to liquids, Int. J. Heat Mass Transfer 13 (5) (1970) 587–753.
[6] R.R. Smith, Characteristics of turbulence in free convection flow past a vertical plate, Ph.D. Thesis, University of London, 1972.
[7] R. Cheesewright, K.S. Doan, Space–time correlation measurements in a turbulent natural convection boundary layer, Int. J. Heat Mass Transfer 21 (7) (1978) 911–921.
[8] M. Miyamoto, H. Kojino, J. Kurima, I. Takanami, Development of turbulence characteristics in a vertical free convection boundary layer, in: Proceedings of the 7th International Heat Transfer Conference, F.R.G., Munich, 1982, vol. 2, pp. 323–328.
[9] K. Kitamura, M. Koike, I. Fukuoka, T. Saito, Large eddy structure and heat transfer of turbulent natural convection along a vertical flat plate, Int. J. Heat Mass Transfer 28 (4) (1985) 837–850.
[10] T. Tsuji, Y. Nagano, Characteristics of a turbulent natural convection boundary layer along a vertical flat plate, Int. J. Heat Mass Transfer 31 (8) (1988) 1723–1734.
[11] T. Tsuji, Y. Nagano, Turbulence measurements in a natural convection boundary layer along a vertical flat plate, Int. J. Heat Mass Transfer 31 (10) (1988) 2101–2111.
[12] T. Tsuji, Y. Nagano, Velocity and temperature measurements in a natural convection boundary layer along a vertical flat plate, Exp. Therm. Fluid Sci. 2 (1989) 208–215.
[13] T. Tsuji, Y. Nagano, M. Tagawa, Thermally driven turbulent boundary layer, in: Proceedings of the 8th Symposium on Turbulent Shear Flows, Munich, vol. 1, 1991, pp. 24.3.1–24.3.6.
[14] Y. Hattori, T. Tsuji, Y. Nagano, N. Tanaka, Turbulence characteristics of natural-convection boundary layer in air along a vertical plate heated at high temperatures, Int. J. Heat Fluid Flow 27 (3) (2006) 445–455.
[15] T. Tsuji, T. Kajitani, Turbulence characteristics and heat transfer enhancement of a natural convection boundary layer in water along a vertical flat plate, in: Proceedings of the 13th International Heat Transfer Conference, Sydney, TRB-08 of CD-ROM, August 2006.
[16] W.M. To, J.A.C. Humphrey, Numerical simulation of buoyant, turbulent flow – I. Free convection along a heated, vertical, flat plate, Int. J. Heat Mass Transfer 29 (4) (1986) 573–592.
[17] R.A.W.M. Henkes, C.J. Hoogendoorn, Comparison of turbulence models for the natural convection boundary layer along a heated vertical plate, Int. J. Heat Mass Transfer 32 (1) (1989) 157–169.
[18] T.W.J. Peeters, R.A.W.M. Henkes, The Reynolds-stress model of turbulence applied to the natural-convection boundary layer along a heated vertical plate, Int. J. Heat Mass Transfer 35 (2) (1992) 403–420.
[19] N. Kasagi, Progress in direct numerical simulation of turbulent transport and its control, Int. J. Heat Fluid Flow 19 (2) (1998) 125–134.
[20] H. Shan, B. Ma, Z. Zhang, F.T.M. Nieuwstadt, Direct numerical simulation of a puff and slug in transitional cylindrical pipe flow, J. Fluid Mech. 387 (1999) 39–60.
[21] M. Piller, E. Nobile, T.J. Hanratty, DNS study of turbulent transport at low Prandtl numbers in a channel flow, J. Fluid Mech. 458 (2002) 419–441.
[22] S. Makino, K. Iwamoto, H. Kawamura, Turbulent structures and statistics in turbulent channel flow with two-dimensional slits, Int. J. Heat Fluid Flow 29 (3) (2008) 602–611.
[23] T.A.M. Versteegh, Numerical simulation of turbulent natural convection between two infinite, differentially heated vertical plates, Ph.D. Thesis, Delft University of Technology, 1998.

[24] T.A.M. Versteegh, F.T.M. Nieuwstadt, A direct numerical simulation of natural convection between two infinite vertical differentially heated walls scaling laws and wall functions, Int. J. Heat Mass Transfer 42 (19) (1999) 3673–3693.
[25] G.N. Coleman, J. Kim, P.R. Spalart, Direct numerical simulation of a decelerated wall-bounded turbulent shear flow, J. Fluid Mech. 495 (2003) 1–18.
[26] M.P. Martin, Direct numerical simulation of hypersonic turbulent boundary layers. Part 1. Initialization and comparison with experiments, J. Fluid Mech. 570 (2007) 347–364.
[27] J.A. Schetz, R. Eichhorn, Unsteady natural convection in the vicinity of a doubly infinite vertical plate, Trans. ASME J. Heat Transfer 84 (1962) 334–338.